Uptake of NO_2 to Deliquesced Dihydroxybenzoate Aerosol Particles

Yulia Sosedova,[†,‡] Aurélie Rouvière,[†] Heinz W. Gäggeler,[†,‡] and Markus Ammann*[,†]

Laboratory for Radio and Environmental Chemistry, Paul Scherrer Institute, 5232 Villigen PSI, Switzerland, Department of Chemistry and Biochemistry, University of Bern, Freierstrasse 3, 3012 Bern, Switzerland

Received: May 29, 2009; Revised Manuscript Received: August 19, 2009

The uptake of nitrogen dioxide (NO_2), a major trace gas in the atmosphere, to deliquesced particles containing the sodium salts of hydroquinone (1,4-dihydroxybenzene) or gentisic (2,5-dihydroxybenzoic) acid was investigated at 40% relative humidity and 23 °C in an aerosol flow tube. The experiments were performed using the short-lived radioactive tracer ^{13}N and a denuder technique. The observed uptake coefficient for NO_2 was up to $\sim 6 \times 10^{-3}$ for the hydroquinone disodium salt aerosol, which exceeds previously reported data in the range 10^{-4} to 10^{-3}. The measured time dependence of NO_2 uptake was fitted using a kinetic model taking into account reactant consumption in the particle phase, and keeping the bulk accommodation coefficient, α_b, and the rate constants for the reaction of dissolved NO_2 with the deprotonated forms of the mentioned phenolic compounds as variables. We obtained $\alpha_b = 0.024^{+0.018}_{-0.003}$ as a best estimate. For gentisic acid, the second-order rate constant was $k_2 = (2.9 \pm 0.1) \times 10^8$ L mol^{-1} s^{-1} and is reported for the first time. The data are consistent with bulk reaction limited uptake, without indications for a surface component in the kinetics.

Introduction

Nitrogen oxides play a central role in tropospheric chemistry. NO_2 is directly produced in small quantities along with NO in processes of fossil fuel combustion, biomass burning, and lightning and by microbial activity in soils. It is also formed in the atmosphere by oxidation of NO with ozone and peroxy radicals.[1] The latter reaction leads to ozone production, since the steady-state O_3 concentration is proportional to the ratio of NO_2 and NO concentrations. The major chemical sink for nitrogen oxides is the reaction of NO_2 with hydroxyl radical, followed by formation and precipitation of nitric acid. Another pathway of removal of nitrogen oxides from the gas phase is by heterogeneous processes, particularly on aerosols of complex organic composition.

Phenolic compounds are ubiquitous in the environment, and in the atmosphere they have been detected in smoke from biomass burning[2] or residential wood fires.[3] Individual molar ratios of these compounds to CO have been estimated on the level of about 10^{-4} in wild fire emissions.[4] In soils, where phenols represent the main building blocks of humic matter, capillary water within the top organic soil layer contains typically between 0.1 and 1 mg L^{-1} of phenolic monomers and about 10 mg L^{-1} of phenols in total (including polyphenols).[5] The wide range of different hydroxy- and methoxy-substituted aromatic compounds is formed in microbial degradation processes and pyrolysis of lignin, one of the major structural components of vegetation. Similar compounds also occur as photo-oxidation products of gas-phase aromatic precursors in the atmosphere.[6] Such phenolic compounds are known scavengers of radicals ($^{\bullet}OH$, $Cl_2^{\bullet-}$ etc.) and excited triplet states of aromatic carbonyls due to their ability to act as electron donating reductants.[7−9] Their presence in the atmosphere may therefore have an important impact on aerosol and heterogeneous chemistry.

Previously it was shown that NO_2 may undergo electron transfer reactions with phenoxide anions in aqueous solutions with a strong pH dependence of the kinetics (for cresols and hydroxybenzenes,[10] catechins,[11] hydroxycinnamic acid derivatives,[12] resorcinol and 2,7-naphthalenediol,[13] guaiacol, syringol and catechol[14]). This behavior was explained in terms of a dramatically different reactivity of neutral phenolic species and phenoxide ions. The corresponding second-order rate coefficients differ by 3 orders of magnitude (10^5 vs 10^8 mol L^{-1} s^{-1}) and depend on the nature and orientation of the substituent.[15] Substituent effects are consistent with electron-withdrawing or -releasing properties of the given substituent and are usually higher in para- than in meta-orientation. Methyl-, methoxy- and hydroxyl-substituted phenols were observed to react faster with NO_2 than unsubstituted phenol, and in the case of halogenated, cyano and nitro derivatives the same reaction was slower.[15]

The role of phenolic species as electron donors to NO_2 as final acceptor has also been suspected to be responsible for the photoenhanced transformation of NO_2 to HONO over humic acids.[16−18] The primary reaction products of gaseous NO_2 with these organics are the corresponding phenoxy type radical and nitrite anion.[19] Phenoxy radicals can undergo polymerization reactions or react with O_2 or NO_2,[20] also contributing to organic nitrates.[21] Nitration products of phenolics that may form in the condensed phase of an aerosol processed by NO_2 or other secondary products evolving from the phenoxy radicals may lead to changes in mass, optical, hygroscopic, or toxic properties of the original aerosol. Therefore, processing of aerosols by NO_2 may have an impact on the climate and health effects of aerosols.

In an acidic aqueous environment, the other primary product, nitrite ion, may be protonated and released to the gas phase as HONO,[22] or undergo secondary chemistry, eventually leading to NO or N_2O.[23,24] In atmospheric chemistry, HONO plays an important role as a OH radical source due to its photolysis.[25] Field studies indicate that HONO is mainly formed heterogeneously from NO_2 on the ground or airborne surfaces such as aerosol particles and cloud droplets. Previous modeling studies have mostly treated the disproportionation of NO_2 on humid

* Corresponding author.
† Paul Scherrer Institute.
‡ University of Bern.

10.1021/jp9050462 CCC: $40.75
Published on Web 09/23/2009

surfaces as a source of HONO. However, the kinetics of this reaction is relatively slow and cannot fully account for the budget of the total HONO concentration in the atmosphere. In environments with a high content of hydroxy-substituted aromatics (such as a biomass burning plume or over exposed soil close to the ground), one can expect the electron transfer reactions with phenolic compounds to be a source of HONO in the gas phase and nitrite in the aerosol phase.[26] On the other hand, it is considered unlikely that the processes studied here represent a significant loss to affect gas-phase NO_2 levels and thus to have a direct impact on the O_3 budget in the atmosphere.

At the more basic level, to understand the behavior of NO_2 in heterogeneous reactions, it is also important to determine the value of the bulk accommodation coefficient α_b, which represents the maximum normalized rate, at which molecules may cross the interface between the gas and the condensed phase. The net uptake of material by the condensed phase is normally smaller, due to solubility limitations or slow reaction in the liquid phase. Hitherto only a few studies have been available on this issue, and the factors limiting the transport of gaseous NO_2 to the liquid phase have remained uncertain. Previous estimates of uptake rates of NO_2 on aqueous surfaces gave relatively low values of uptake coefficients (10^{-4} to 10^{-3}),[27−30] down to $<10^{-7}$ for pure water[14] and sulfuric acid solutions.[31] Some of these studies aimed at determining α_b and suspected a surface reaction of NO_2,[22,32] while others showed that they had mainly bulk reaction (hydrolysis) limited uptake.[30] However, in these studies no significant aqueous-phase sink other than hydrolysis was present to allow driving the system possibly into bulk accommodation limitation. Lee and Tang (1988)[33] measured NO_2 uptake on alkaline hydroquinone solutions in a stop-flow reactor combined with a gas-phase absorption technique and reported a value of $(6.3 \pm 0.7) \times 10^{-4}$ for the bulk accommodation coefficient and suggested that this may limit interfacial mass transport of NO_2 into cloud or fog droplets.

In this study, we attempt to get an improved estimate for α_b by using an aerosol flow tube, where reaction conditions could be better characterized. Hydroquinone and gentisic acid were chosen as model compounds, because as already mentioned, they show enhanced reactivity toward NO_2 in the form of phenoxide ions. For gentisic acid, the reaction with NO_2 has not been investigated before.

Experimental Section

The short-lived radioactive tracer technique is an effective and sensitive method to study heterogeneous kinetics under realistic conditions. It allows performing experiments at very low concentrations of a trace gas. Another advantage of this method is the possibility to do measurements in the presence of water, which interferes negatively in several other techniques of trace gas measurements, such as IR or mass spectrometry. The amount of water in all phases is very crucial for the reactivity of aerosols, because it defines the phase state of the particles and possibly the mechanism. These features allow experiments with aerosol particles at humidity and pressure relevant to the real atmosphere.

Production of Labeled $^{13}NO_2$. The isotope ^{13}N with a half-life $\tau_{1/2} = 10$ min is a well-known positron emitter and has been widely used to label molecules in space and time in positron emission tomography for medical applications. Nevertheless, only very few studies have used the short-lived radioactive tracer ^{13}N for the investigation of gas−solid or gas−liquid interactions in atmospheric chemistry. A facility for the online production of ^{13}N labeled nitrogen monoxide has been used at the Paul Scherrer Institute, Switzerland, for many years, as described in detail elsewhere.[34,35] In brief, the ^{13}N isotope is produced via the reaction of ^{16}O with 11 MeV protons in a gas-target, which is essentially a small quartz coated flow reactor, in a continuous mode. ^{13}N rapidly forms highly oxidized and reactive forms of nitrogen oxides. To minimize the wall losses during the long-distance transport through tubes, they are chemically converted to ^{13}NO (nitrogen monoxide) over a Mo converter attached to the main body of the target. Note that the radiation chemistry in the target cell also leads to the production of nonlabeled nitrogen oxides at around 30 ppbv from nitrogen impurities in the carrier gas supplies as well as to the formation of carbon monoxide, carbon dioxide and possibly other small organic molecules from organic impurities at similar levels.

The gas mixture containing labeled ^{13}NO was continuously delivered to the laboratory through a 580 m long, 4 mm inner diameter PVDF tube. There, it was diluted with N_2 and mixed with a certified amount of nonlabeled NO to cover the concentration range from a few ppb to several hundred ppb. As a byproduct of the proton irradiation of the gas target, the short-lived isotope ^{11}C could also be observed, presumably formed from the reaction of carbon present as contamination in the carrier gas and on the surfaces of the target housing with secondary neutrons. To get rid of possible ^{11}C labeled organic compounds and carbon monoxide, the target gas was passed through a CuO converter at 800 °C. The resulting CO_2 was trapped over 6 mm i.d. glass balls covered with NaOH. No CO_2 could be detected after that with a CO_2 gas analyzer (model 41C Trace Level), and no sign of the ^{11}C isotope (with a half-life $\tau_{1/2} = 20$ min) was observed in radioactive decay analysis performed routinely during the experiments.

To convert NO to NO_2, surface oxidation over firebrick granules impregnated with CrO_3 was used.[34,36] This conversion has better efficiency under humid conditions, and the gas flow was humidified before. For that it was passed through a vertically mounted Gore-Tex tube partially immersed in water. By varying the water level, we could adjust the resulting humidity measured by a capacitance humidity sensor between 5 and 80%. Trace amounts of HONO produced were absorbed in a sand-blasted glass tube coated with Na_2CO_3 prior to entering the reactor. This procedure leads to an almost complete conversion of NO to NO_2 as routinely monitored with a commercial NO/NO_x analyzer (Monitor Laboratories ML 9841). The total amount of radioactivity in the gas phase serving as a reference is also measured prior to the reactor.

Aerosol Production. In a first step, deliquesced particles were produced by mixing and nebulizing aqueous solutions of sodium hydroxide (NaOH) and of hydroquinone (HQ, Fluka, ≥99%) or gentisic acid (GA, Sigma-Aldrich, 98%), into a flow of nitrogen. Milli-Q water was always used for nebulized solutions. Because we expected the solutions of the sodium salts of these compounds to be very reactive toward any oxidant present in room air, the two solutions were pumped separately with peristaltic pumps and mixed immediately before the nebulizer. The concentration of 0.2 mol L^{-1} was kept fixed for the NaOH solution (8 g L^{-1}) in all experiments, whereas the concentration of the organic constituents was varied. The maximum amount of 11 g L^{-1} for HQ and 10.3 g L^{-1} for GA was chosen such that all of the hydroxy groups were expected to be deprotonated in the mixture with 0.2 mol L^{-1} NaOH solution (i.e., we assumed to produce hydroquinone disodium and gentisic acid trisodium salts, Na_2HQ and Na_3GA, correspondingly). To decrease the total GA concentration, malonic acid (MA, Sigma-Aldrich, 99%) was added as a nonreactive matrix to match the

TABLE 1: GA and HQ Bulk-Phase Concentrations in Aerosols, Prepared by Mixing and Nebulizing Equal Amounts of Solutions 1 and 2 at 40% RH

			solution 1	solution 2		
aerosol no.	reactive molecule Ar	molar ratio NaOH:Ar x:1	m(NaOH), g L^{-1}	m(Ar), g L^{-1}	m(MA), g L^{-1}	$[Ar]_b$, mol L^{-1}
1	GA	3	8	10.3	0	4.3
2	GA	7.4	8	4.2	6.1	1.7
3	GA	12.5	8	2.5	7.9	1
4	GA	30	8	1.0	9.4	0.4
5	GA	120	8	0.3	10.1	0.1
6	GA	300	8	0.1	10.3	0.04
7	HQ	3	8	7.3	3.5	4
8	HQ	2	8	11.0	0	4

total amount of acid protons equal to that in the solution with the highest concentration of GA. No water activity data are available for the solutions relevant for the conditions of the experiments. Therefore, to estimate the real concentration of the organics in the aerosol, saturated solutions of GA, MA, and NaOH mixtures in ratios as used in the experiments were prepared. Then, the solutions were left in a box under a flow of N_2 at 40% of relative humidity (the RH at which most of the experiments were performed) overnight to get them into equilibrium. From the change in mass before and after the equilibration, the equilibrated bulk concentration at 40% relative humidity of the compounds as well as the amount of water was calculated. The bulk-phase concentrations of total GA estimated in such a way for the different aerosol types are presented in Table 1.

The primary droplets exiting the nebulizer are initially dried by passing the flow through a diffusion dryer filled with silica gel. To avoid uncontrollable wall losses of charged particles, which are typically produced when nebulizing a solution, they are removed by passing the aerosol flow first through an ^{85}Kr source (a bipolar ion source), where an equilibrium charge distribution is attained, and then through an electrostatic precipitator. After being neutralized, the aerosol flow is conditioned to the relative humidity of interest (20−75% RH) by passing it through a vertically mounted Gore-Tex tube partially immersed in water. To allow complete deliquescence, the aerosol is passed through an equilibration chamber with about 1 min residence time before entering the aerosol flow tube.

The determination of the total aerosol surface to volume ratio is critical for an accurate evaluation of the uptake coefficient and was performed with a Scanning Mobility Particle Sizer (SMPS) consisting of an ^{85}Kr source to re-establish charge equilibrium on the aerosol, and a differential mobility analyzer (DMA) coupled to a condensation particle counter (CPC, TSI 3022). The same relative humidity was maintained both in the DMA sheath gas and in the aerosol flow tube (by using filtered carrier gas from the flow tube as sheath gas in the DMA), since the aerosol liquid water content and consequently the particle diameter and the aerosol surface to volume ratio strongly depend on the relative humidity. The other method used to monitor the total surface area of the aerosol consisted of first charging the particles by an ^{85}Kr source and then measuring the current created by the charged particles of one polarity precipitated due to the electric field in an annular condenser, to which a voltage of 3000 V was applied. This device is further referred to as E-filter. The E-filter allowed monitoring aerosol surface concentration with a time resolution of several seconds, but it did not measure it in absolute values and was calibrated against SMPS data. The aerosol normally produced in our experiments had a log-normal distribution with a mode diameter of about 100 nm and a typical surface to volume ratio in the range of $(7-11) \times 10^{-2}$ m^2 m^{-3}, depending on the relative humidity and the content of the nebulized solution.

Flow Tube for Kinetic Experiments. The aerosol and NO_2 containing flows were mixed in a cylindrical flow tube reactor. The reactor is a glass tube of 1.95 cm inner diameter lined with a PFA foil to minimize the effect of NO_2 retention and loss on the wall. Note that after removal of charged particles prior to the flow reactor (see above) the losses of particles to the walls are minimized and not detectable by the SMPS system. No significant losses of NO_2 on the walls were observed in our experiments, except after extensive exposure of the flow tube to aerosol particles. Therefore, to avoid an effect of particles residing on the walls, the PFA foil was replaced before every new experiment.

The gaseous NO_2 was introduced to the flow reactor via a movable injector along the axis, while the aerosol gets into the annular space between the injector and the flow tube through a T-connector. The position of the injector determines the duration of the gas-aerosol interaction, and reaction times between approximately 1 and 60 s could be achieved. There are lateral pinholes at the tip of the injector, through which the gas enters the flow reactor perpendicular to the flow of the aerosol. This design facilitates rapid mixing of the flows, which is critical for exactly controlling the reaction time. The temperature in the reactor and the whole flow system was kept constant at 296 K by making use of the efficient temperature controlled air conditioning system in the laboratory. This led to better results than trying to control the temperature of the flow tube, the SMPS system and the analysis system (see below) separately. The pressure in the system was typically 960−990 mbar. The relative humidity of the gas flow was continuously measured downstream of the reactor.

Detection System. After leaving the reactor, the gas flow directly entered a parallel-plate denuder system to separate the gaseous species HONO and NO_2 on different chemically selective coatings by lateral diffusion (Figure 1). The submicrometer aerosol particles have a small diffusivity and pass through the denuder

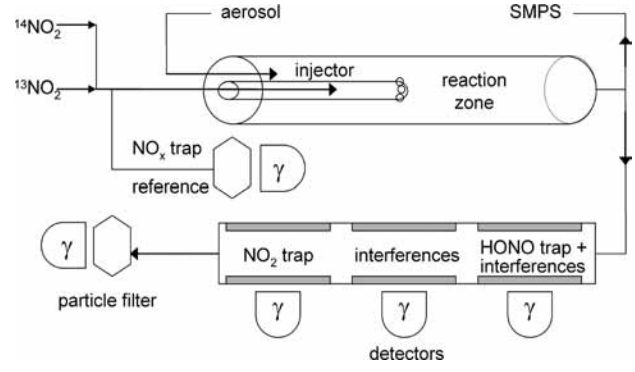

Figure 1. Scheme of the experimental setup.

without being collected. Gaseous nitrous acid was taken up in the first denuder section (a pair of denuder plates 10 cm long) coated either with a 1.4% solution of Na_2CO_3 in 50% methanol/water or with a 4:1 mixture of 1% sulfanilamide (SA, Sigma-Aldrich, ≥99%) in methanol and 2 mol L^{-1} H_2SO_4 solution, respectively, and subsequently dried under N_2 flow. To exclude interferences with NO_2, the Na_2CO_3 or SA coating is repeated in the second section. The third section is covered with a solution of 1% *n*-(1-naphthyl)diethylenediamine dihydrochloride (NDA, Fluka, ≥99%), 1% KOH, and 10% water in methanol and then dried to react with NO_2. NDA forms part of the Saltzman reagent[37] and reacts rapidly with NO_2. The basic coating assures that the nitrite product stays on the surface. All coatings were freshly prepared before each new experiment. After passing the denuder with almost 100% efficiency, the aerosol particles were retained in a glass fiber filter. An additional glass-fiber filter soaked with a mixture of NDA and KOH and dried was used to monitor the total concentration of ^{13}N labeled gaseous NO_2 before entering the reactor by diverting a small gas flow containing the NO_2 just upstream of the injector through this filter. This measurement provides a reference for the generation of NO_2 and allows recognizing and eventually correcting for variations of the flux of ^{13}N arriving in the laboratory.

The decay of ^{13}N atoms results in emission of a positron, which, upon annihilation with an electron, results in the coincident emission of two γ-rays in opposite directions. A CsI scintillator crystal with integrated PIN diode (Carroll and Ramsey Associates, Model 105) was attached to each trap (denuder sections and filters) to detect the amount of emitted γ quanta. The counts of γ-decays integrated within 1 min, equivalent to the amount of ^{13}N-labeled molecules of a given species, was recorded and converted to the flux of these molecules into the corresponding denuder trap or particle filter by the inversion procedure reported earlier.[38−40] The flux into trap *j*, I_j, can be derived from the difference between two consecutive activity measurements, $A_{j(i-1)}$ and $A_{j(i)}$, recorded at times $t_{(i-1)}$ and t_i, according to eq 1, where λ is the decay constant of ^{13}N ($\lambda = 0.00116\ s^{-1}$):

$$I_j = \frac{A_{j(i)} - A_{j(i-1)} \exp(-\lambda(t_{(i)} - t_{(i-1)}))}{1 - \exp(-\lambda(t_{(i)} - t_{(i-1)}))} \qquad (1)$$

This flux is proportional to the total amount of ^{13}N-labeled molecules absorbed at a specific denuder plate or filter per unit time, i.e., to the concentration of the corresponding species, which is used for the calculation of the uptake coefficient.

The relative counting efficiency of each γ-detector is determined by accumulating a certain amount of $^{13}NO_2$ on the "reference" filter and exposing it in turn to each of the other detectors in a way that closely mimics the geometrical configuration at each trap. Further details of the preparation of the coatings, traps and filter efficiencies, and the performance of the detection system were published elsewhere.[34,38]

pK_a Determination. Because phenoxide type ions react with NO_2 much faster than neutral phenolic species,[10−12] it is important to know the degree of deprotonation of the phenolic groups in aqueous solutions pertaining to our experiments. For HQ, the values of pK_a (at 25 °C) were taken from the literature (pK_{a1} = 9.85, pK_{a2} = 11.4),[41] whereas the data for GA were only available for the deprotonation of the carboxylic group at 25 °C: pK_{a1} = 2.97,[41] 2.93,[42] 2.89 ± 0.04.[43] To determine the dissociation constant for phenolic groups of GA, a UV−Vis spectroscopic technique was applied. The main idea is that molecular forms with different amounts of protons have different

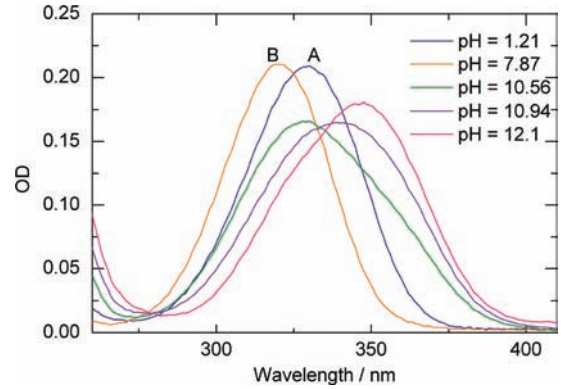

Figure 2. Optical absorption spectra of GA aqueous solutions at different pH, with spectrum A belonging to neutral GA and spectrum B to GA with the dissociated carboxylic group.

absorption spectra. By changing the pH of the solution, one changes the relative abundance of the species. This method has been used before for other species.[44−46]

A solution of GA (Sigma, puriss. p.a.) in pure Milli-Q water has an absorption maximum at 320 nm (Figure 2). This long-wave absorption band corresponds to the π—π^*-transition, which is characteristic of all salicylic acid derivatives,[47] and its position usually depends on the pH of the solution. A series of absorption spectra was recorded after stepwise titration of a sodium hydroxide solution containing ~5.5×10^{-6} mol L^{-1} GA with small amounts of concentrated hydrochloric acid at 23 °C. The quartz cuvette with the sample was continuously deoxygenated, and the pH of the solution was measured every time after addition of the acid. For pH below 7.8 optical spectra were treated as a superposition of spectra of only two molecular forms of GA, the neutral (A) and that with the carboxylic group dissociated (B) (Figure 2). A spectrum for the pure A form was recorded at pH = 1.2, and for B at pH = 7.8. To find the relative abundances of these two forms, the MATLAB lsqcurvefit optimization function was used. The fits were fairly well constrained, and the error was not higher than 5%. Calculated relative abundances were plotted versus pH, and from the titration curves obtained a value for the dissociation constant was determined. The pK_{a1} = 2.92 ± 0.03 was in very good agreement with the literature values for the dissociation of the carboxylic group in GA cited above. The dissociation constants of both hydroxy groups, K_{a2} and K_{a3}, were determined using graphic linearization methods described by Blanco et al.,[46] because their values lie close together and the absorption spectra substantially overlap. The left part of eq 2 was plotted vs A_λ, the absorbance at selected wavelength (330 and 349 nm were chosen), for optical spectra of GA in the pH range 5.9−11.5, where A_{λ,H_2GA^-} is the absorbance of H_2GA^-, recorded at the same wavelength at pH = 7.8. From the slope the value of pK_{a2} = 10.4 ± 0.1 and from the intercept with the *y*-axis the absorbance of HGA^{2-}, A_{λ,HGA_2^-}, were found. The latter was substituted to eq 3, with A_{λ,GA_3^-} being the absorbance of GA^{3-}, and an analogous plot in the pH range 12.1−13.2 was done to determine pK_{a3} = 12.5 ± 0.1.

$$(A_\lambda - A_{\lambda,H_2GA^-}) \times 10^{-pH} = -K_{a2}A_\lambda + K_{a2}A_{\lambda,HGA^{2-}} \qquad (2)$$

$$(A_\lambda - A_{\lambda,HGA^{2-}}) \times 10^{-pH} = -K_{a3}A_\lambda + K_{a3}A_{\lambda,GA^{3-}} \qquad (3)$$

Both dissociation constants of the hydroxylic groups are lower than those of HQ and resorcinol (9.2, 10.9),[46] which could be

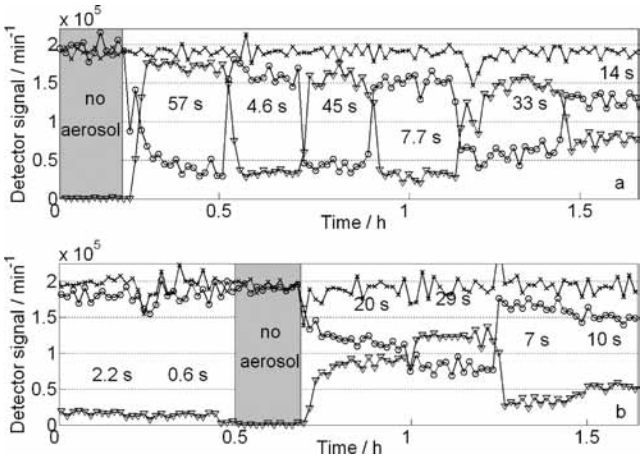

Figure 3. Experimental profiles of NO_2 interacting with aerosol 1, containing Na_3GA (a), and aerosol 8, containing Na_2HQ (b): (circles) NDA denuder signal (representing gas-phase NO_2); (triangles) signal from particle filter (particulate nitrite or other product); (asterisks) from reference filter. The aerosol surface area was 0.093 and 0.062 $m^2\ m^{-3}$, and the initial NO_2 mixing ratio was 7.7 and 19 ppbv, respectively. Numbers in seconds represent the corresponding reaction times; gray areas indicate the periods during which no aerosol was in the reactor.

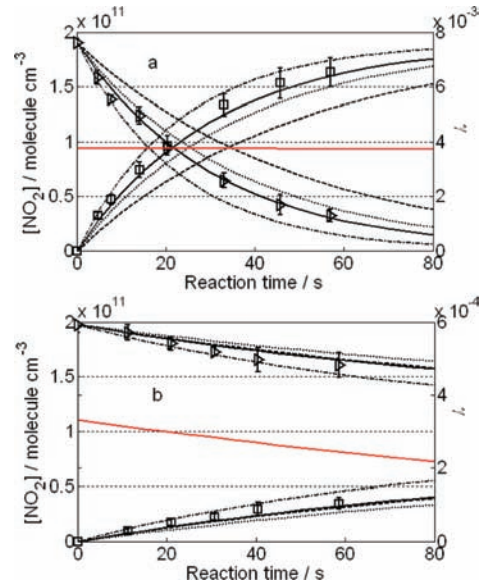

Figure 4. Kinetic curves of NO_2 uptake on aerosols 1 (a) and 6 (b): (triangles) experimental data points for NO_2 in the gas phase; (squares) those for products carrying labeled nitrogen on particles (with 2σ uncertainties); (lines) model simulation (see below) with $\alpha_b = 0.024$ and $k_2 = 2.9 \times 10^8$ L mol^{-1} s^{-1} (solid lines), $k_2 = 2 \times 10^8$ L mol^{-1} s^{-1} (dotted lines), $k_2 = 6 \times 10^8$ L mol^{-1} s^{-1} (dash-dotted lines) and with $\alpha_b = 0.005$ and $k_2 = 2.9 \times 10^8$ L mol^{-1} s^{-1} (dash lines). Red lines represent uptake coefficients for $\alpha_b = 0.024$ and $k_2 = 2.9 \times 10^8$ L mol^{-1} s^{-1} (right y-axes). $[GA]_g$ is (a) 365 ppbv $\gg$ initial $[NO_2]_g = 7.7$ ppbv and (b) 3.5 ppbv < initial $[NO_2]_g = 8$ ppbv.

explained by formation of an intramolecular hydrogen bond between the carboxylic and OH group in the ortho position.[48] The pK values were used to calculate the degree of deprotonation of phenolic groups in the nebulized solutions. For aerosol 1 and aerosols 7 and 8 the main species in solution were Na_3GA and Na_2HQ, respectively. For aerosols 2−6 the mole fraction of the fully deprotonated Na_3GA was decreased from 87% to 42%, and the fraction of NaH_2GA increased from 13% to 58% with increasing MA concentration in nebulized solutions. Thus in all our experiments the reactive molecule had at least one deprotonated phenolic group. Note that there is some uncertainty in this extrapolation of dilute solution behavior to the high ionic strength solution of the deliquesced aerosol particles of our experiments.

Results and Discussion

In a series of experiments the uptake of gaseous NO_2 on aerosols containing gentisic acid tri- and disodium salt (Na_3GA and NaH_2GA) or hydroquinone disodium salt (Na_2HQ) was measured at different total bulk-phase concentrations of aromatic species, $[Ar]_b$ (Table 1). For most of these experiments a relative humidity of 40 ± 3% and an initial gas-phase concentration of ~8 ppbv of nonlabeled NO_2 were chosen. Some experiments were also performed at different initial NO_2 concentrations. Kinetic experiments usually involved measurements of the uptake of NO_2 at eight different contact times in the range 0−60 s (0−88 cm injector displacements).

Typical experimental profiles are presented in Figure 3. In the absence of aerosol (peristaltic pumps supplying the solutions to the nebulizer switched off), only a signal on the NDA denuder was observed, while the signal at the particle filter remained at the detection limit (gray areas in Figure 3). Under given conditions (reactor covered with PFA foil, 40% RH, 8 ppbv of NO_2), there was no change in the NO_2 signal, when the injector was pulled in from the maximum injector position to the minimum. This indicated that there was no wall loss by retention or reaction and that the level of the initial NO_2 concentration, $[NO_2]_g(t=0)$, was equal for each injector position. While a fraction of 1−10% of the NO_2 signal was observed at the carbonate (or sulfanilamide) denuder, in most of the experiments no difference in the signals from the first and the second of these denuders was observed either at the beginning or at the end of a series of experiments. This indicated that HONO levels were below detection limits in our system. Finally, particles were admitted to the reactor by switching on the peristaltic pumps, which led to a decrease in the gas-phase NO_2 signal and the appearance of a ^{13}N signal on the particle filter. It was an indication that a fraction of the labeled $^{13}NO_2$ molecules had been taken up by the aerosol. To study the reaction kinetics, the contact time between gaseous NO_2 and aerosol was varied by changing the position of the injector. Aerosol production was switched off either after a few movements of the injector as shown in Figure 3 or at each injector position, especially at lower concentrations to be sure to capture a well-defined aerosol off initial level for NO_2. As shown in Figure 3, the signal from the particle filter increased with increasing injector position, i.e., reaction time.

To minimize the statistical error, we usually recorded saturating signals I_j from denuders and the particle filter at the same injector position, i.e., reaction time t, for 10−15 min. I_j were then averaged within these steady-state periods, and the mean values for the concentrations of NO_2 in the gas phase, $[NO_2]_g(t)$, and its daughter product in the particulate phase, referred to as $[NO_2]_p(t)$, were calculated for each reaction time t. Examples for the kinetic curves obtained by this way are presented in Figure 4 (experimental data points).

Kinetic curves for uptake of NO_2 to aqueous aerosols produced from the mixtures given in Table 1 were measured at different conditions. It was found that the rate of NO_2 uptake was dependent on the total gentisic acid bulk concentration, $[GA]_b$, as demonstrated with the relative NO_2 consumption for the case of aerosol 3. The rate of uptake was independent of the NO_2 concentration below 20 ppbv, when the overall GA

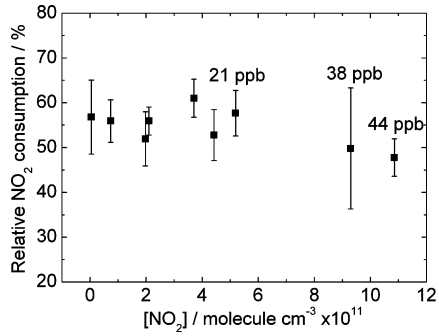

Figure 5. Relative consumption of NO_2 in presence of aerosol 3 as a function of the NO_2 gas-phase concentration, calculated by dividing the difference between the initial signal from the NDA denuder and this signal after the exposure of NO_2 to an aerosol at the injector position at 88 cm, corresponding to 1 min, by the initial signal. $[GA]_g$ was 80 ppbv. NO_2 uptake is normalized to the aerosol surface area.

concentration in the reactor, i.e., $[GA]_g = [GA]_b V_b$, where V_b is the particle bulk volume per volume of aerosol, was 80 ppbv (Figure 5), i.e., under conditions of GA excess. When the overall concentration of NO_2 in the reactor was comparable to or larger than the GA concentration, significant depletion of GA in the bulk aerosol phase occurred within the reaction time. The onset of this behavior is appearing as the slightly lower relative consumption in Figure 5 at larger NO_2 concentration. This effect was expected to be more pronounced for the mixtures with lower GA concentrations but was not investigated further in this form.

Therefore, especially for aerosol composition with low GA concentration, even for the lowest NO_2 concentrations applied, GA was not in excess anymore. This is demonstrated with the data shown in Figure 6. Conditions used on the upper plot (Figure 6a) correspond to the case of relatively low initial NO_2 concentration (initial $[NO_2]_g = 7.7$ ppbv $\ll [GA]_g = 365$ ppbv), and experimental data points plotted in logarithmic scale could be fitted linearly through the data covering the complete range of reaction times. Apparently the uptake kinetics in this case

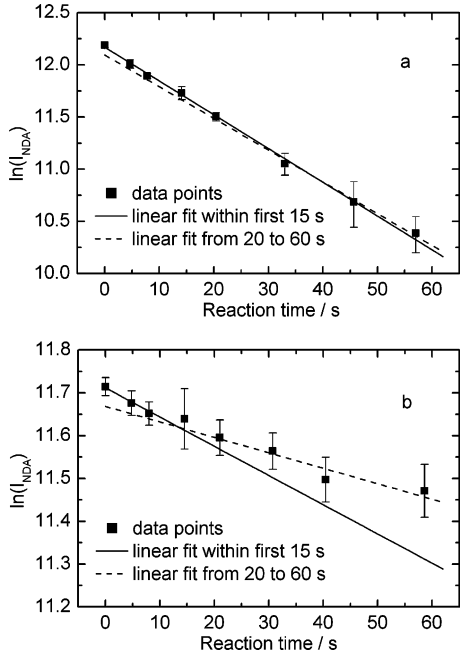

Figure 6. Logarithmic NDA denuder signals during the interaction of NO_2 with aerosols 1 (a) and 5 (b) and linear fits (solid lines) within first 15 s (4 first data points) and (dashed lines) from 20 to 60 s (4 later points).

could be considered to be of first order, and the slope corresponds to a pseudo-first-order loss rate coefficient k_p:

$$\frac{d[NO_2]_g}{dt} = -k_p[NO_2]_g \tag{4}$$

k_p can be used to calculate the uptake coefficient γ, which is the probability that a gas kinetic collision actually results in loss of the molecule in the bulk aerosol phase, via

$$\gamma = \frac{4k_p}{S\omega} \tag{5}$$

where S is the aerosol surface concentration ($m^2\ m^{-3}$) measured during the experiment with the SMPS system and ω is the mean thermal velocity ($m\ s^{-1}$) of NO_2 molecules, given as

$$\omega = \sqrt{\frac{8RT}{\pi M}} \tag{6}$$

with R, T, and M being the gas constant, the absolute temperature and the molar weight of NO_2, respectively. For Figure 6a eq 5 leads to $\gamma = (4.3 \pm 0.3) \times 10^{-3}$. On the other hand, for the data shown in Figure 6b (initial $[NO_2]_g \sim [GA]_g \sim 8$ ppbv) a change in slope is apparent, when data within the first 15 s or only data from 20 s up to 60 s are considered. This would indicate a decrease of γ from initially $(8.6 \pm 4.4) \times 10^{-4}$ by a factor of almost 2 to $(4.6 \pm 2.4) \times 10^{-4}$. We therefore developed a more explicit kinetic model to keep track of the GA bulk-phase concentration to allow extracting the elementary kinetic parameters.

For NO_2 uptake to the liquid particles containing GA or HQ molecules, the net uptake coefficient can be represented by eq 7, if we assume that reactive loss of NO_2 occurs by reaction with GA or HQ in the bulk of the particles:

$$\frac{1}{\gamma} = \frac{1}{\alpha_b} + \frac{1}{\Gamma_b} \tag{7}$$

where Γ_b is the limiting uptake coefficient due to reaction in the bulk phase of the particles and α_b is the bulk accommodation coefficient, which is the probability that a molecule colliding with the surface is entering the liquid phase.[49] For small droplets of radius r_p, the concept of the reacto-diffusive length is important. This is the characteristic distance beyond the surface of the particle, within which an NO_2 molecule is lost by reaction and is given by eq 8, where D_{b,NO_2} is the NO_2 bulk diffusion coefficient ($1.23 \times 10^{-5}\ cm^2\ s^{-1}$),[30] k_2 is a second-order rate coefficient ($L\ mol^{-1}\ s^{-1}$), and $[Ar]_b = [GA]_b$ or $[HQ]_b$ in mol L^{-1}.

$$l = \sqrt{\frac{D_{b,NO_2}}{k_2[Ar]_b}} \tag{8}$$

For typical aerosol particles with radius ~50 nm, $[GA]_b$ concentration in the range 0.04−4.3 mol L^{-1}, and $k_2 = 10^8$ L $mol^{-1}\ s^{-1}$, l is in the range 2−20 nm. Using the known second-order rate coefficient for HQ, $k_2 = 1.1 \times 10^9$ L $mol^{-1}\ s^{-1}$, leads to smaller l in the range 0.3−3.6 nm.

If $l \gg r_p$, the reactivity becomes bulk volume limited, while in the other case (the more frequent one), the reaction is confined to a thin layer of thickness l near the surface and is therefore limited by the surface area, and the uptake coefficient is given by

$$\Gamma_b = \frac{4HRT}{\omega}\sqrt{D_{b,NO_2}k_2[Ar]_b} \quad (9)$$

with H being the Henry's law coefficient (mol atm^{-1} L^{-1}).

For the transition between the two regimes, for spherical particles, the following equation can be used:[50]

$$\Gamma_b = \frac{4HRT}{\omega}\sqrt{D_{b,NO_2}k_2[Ar]_b}\left[\coth\left(\frac{r_p}{l}\right) - \left(\frac{l}{r_p}\right)\right] \quad (10)$$

For particles used in our experiments l was expected to be between 0.5 and 20% of r_p depending on $[GA]_b$, and up to 40% of r_p for aerosols 5 and 6. The deviation from eq 9 was significant, and we therefore used eq 10 for all further calculations of Γ_b.

Considering that pseudo-first-order loss from the gas phase is equal to eq 4, a system of differential equations can be written:

$$\frac{d[NO_2]_g}{dt} = -\frac{0.25S\omega}{\frac{1}{\alpha_b} + \frac{1}{\Gamma_b}}[NO_2]_g$$

$$\frac{d[Ar]_g}{dt} = -\frac{0.25S\omega}{\frac{1}{\alpha_b} + \frac{1}{\Gamma_b}}[NO_2]_g \quad (11)$$

$$[Ar]_g = [Ar]_b\frac{V_b}{V}$$

The system of eqs 11 was solved numerically using the solver ODE23 MATLAB (Version 7.6.9. (R2008a)). The differential eqs 11 were integrated over a time period from 0 to 100 s with the initial concentrations $[NO_2]_g(t=0)$ and $[Ar]_b(t=0)$ taken from the experiment. All parameters were known from the experiments except for k_2 and α_b. Numerical solutions for $[NO_2]_g$ and $[NO_2]_p = [NO_2]_g(t=0) - [NO_2]_g$ were used to fit the experimental data (Figure 4, lines on the upper graphs). k_2 and α_b were taken from the best fits.

First we applied our model to analyze the data on NO_2 uptake to the aerosol containing HQ (aerosols 7 and 8, $[NO_2]_g(t=0) =$ 7−19 ppbv). Because of the relatively high bulk uptake rate Γ_b, the loss of the gas-phase NO_2 is strongly affected by the bulk accommodation coefficient α_b, making it possible to estimate the value of the latter. The evaluation of three available data sets with both k_2 and α_b as variable parameters gave $\alpha_b =$ 0.025 and $k_2 = 11.3 \times 10^8$ L mol^{-1} s^{-1} (Table 2). The latter corresponds exactly to the literature value.[15] To estimate errors for each individual experiment, we simulated N data sets with randomized deviation from the observed experimental data set with known standard deviation. After the program fitted N data sets, asymmetric distributions for α_b and k_2 were returned, with longer tails toward higher values for α_b (Figure 7) and vice versa for k_2. Therefore, we present $k_2 = 11.3^{+0.2}_{-1.4} \times 10^8$ L mol^{-1} s^{-1} with asymmetric errors, standing for the 95% confidence interval (2.5% of the values from both sides of the α_b distribution histogram were omitted).

TABLE 2: Second-Order Rate Constant k_2(obs) and Bulk Accommodation Coefficient α_b Derived from the Kinetic Model Applied to the Data from Different Experiments of NO_2 Interaction with GA or HQ Aerosols[a]

aerosol #	k_2(obs), 10^8 mol $L^{-1}s^{-1}$	α_b	$\gamma_0 \times 10^3$
1	$2.9^{+0.3}_{-1.1}$	$0.015^{+0.055}_{-0.004}$	$3.1^{+1.3}_{-0.6}$
	$3.1^{+0.2}_{-0.4}$	$0.033^{+0.035}_{-0.009}$	$4.0^{+0.5}_{-0.3}$
	$3.0^{+0.4}_{-0.7}$	$0.019^{+0.033}_{-0.006}$	$3.7^{+0.7}_{-0.6}$
2	$3.2^{+0.1}_{-0.2}$		$2.6^{+0.1}_{-0.1}$
	$2.3^{+0.2}_{-0.2}$		$2.2^{+0.1}_{-0.1}$
3	$2.6^{+0.2}_{-0.3}$		$1.8^{+0.1}_{-0.1}$
	$3.3^{+0.2}_{-0.2}$		$2.1^{+0.1}_{-0.1}$
4	$2.7^{+0.1}_{-0.1}$		$1.2^{+0.1}_{-0.1}$
5	$3.3^{+0.3}_{-0.4}$		$0.64^{+0.05}_{-0.03}$
6	$4.1^{+0.6}_{-0.7}$		$0.41^{+0.04}_{-0.03}$
median	$2.92^{+0.06}_{-0.08}$		
7	$11.3^{+0.3}_{-0.5}$	$0.029^{+0.009}_{-0.004}$	$6.6^{+0.3}_{-0.3}$
8	$11.6^{+0.4}_{-1.1}$	$0.018^{+0.010}_{-0.006}$	$5.6^{+1.7}_{-1.0}$
	$10.7^{+0.8}_{-3.7}$	$0.027^{+0.046}_{-0.005}$	$6.3^{+1.4}_{-1.2}$
median	$11.3^{+0.2}_{-1.4}$	$0.024^{+0.018}_{-0.003}$	

[a] k_2(obs) and α_b parameters were obtained by fitting simulated uptake curves to experimental data points, as explained in the text. For experiments with GA aerosols 2−6, α_b was fixed at 0.024. The initial net uptake coefficients γ_0 were calculated using k_2(obs) and initial GA or HQ concentration.

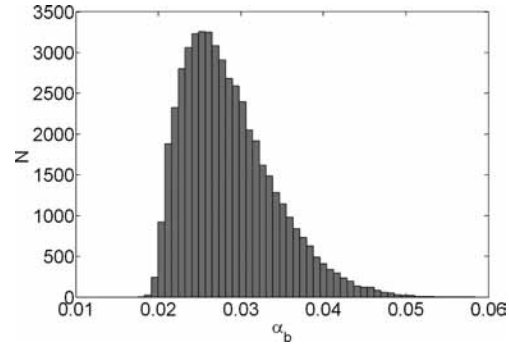

Figure 7. Asymmetrical distribution for α_b.

For NO_2 uptake to the aerosol containing GA, the experimental data cover cases in which $[GA]_b$ was high and cases in which significant depletion of GA occurred during the residence time in the flow reactor, as discussed above. In the case of large GA concentrations, the loss of the gas-phase NO_2 is again sensitive to the bulk accommodation coefficient. This is demonstrated in Figure 4a, showing that variation of the α_b from 0.024 to 0.005 leads to a dramatic change in the loss and gain curves. For the other case, the loss of NO_2 from the gas phase is determined by the liquid-phase rate constant k_2 and the depletion of liquid-phase GA molecules, i.e., for α_b between 10^{-2} and 1, $1/\alpha_b \ll 1/\Gamma_b$. The data shown in Figure 4b then allow estimating k_2 to lie in the range $(2-6) \times 10^8$ L mol^{-1} s^{-1}. But as discussed in the Experimental Section, the fraction of fully deprotonated GA decreased from aerosol 1 to aerosol 6. Thus in aerosol 1, the reactivity can be attributed entirely to Na_3GA with corresponding $k_2(Na_3GA)$, while in aerosol 6 both forms Na_3GA (40%) and Na_2HGA (60%) are reactive. Taking into account the estimated fraction of Na_3GA in aerosol 6, the following condition should be fulfilled: $0.4k_2(Na_3GA) < k_2$(obs), where k_2(obs) is an apparent overall second-order rate constant observed in the experiment with aerosol 6. For simulations with α_b below 7.5×10^{-3} this condition could not be satisfied. At $\alpha_b = 7.5 \times 10^{-3}$ $k_2(Na_3GA)$ should be 1.1×10^9 L mol^{-1} s^{-1}

and $k_2(\text{obs}) = 4.4 \times 10^8$ L mol^{-1} s^{-1} to bring the simulation into agreement with observations; therefore, $k_2(Na_2HGA)$ should be at least 2 orders of magnitude less than $k_2(Na_3GA)$. For, e.g., $\alpha_b = 0.01$, $k_2(Na_3GA) = 6.5 \times 10^8$ L mol^{-1} s^{-1} and is only twice as high as $k_2(Na_2HGA) = 2.7 \times 10^8$ L mol^{-1} s^{-1}, which is comparable to the difference in reactivity between the HQ mono-ion ($k_2 = 9.0 \times 10^8$ L mol^{-1} s^{-1}) and dianion ($k_2 = 1.7 \times 10^9$ L mol^{-1} s^{-1}) toward ClO_2.[51] For $\alpha_b > 0.02$ no difference in reactivity of both forms is needed to explain the experimental data. pH dependent measurements with constant GA concentrations would be needed to constrain better the difference in reactivity for the two forms. To give a more precise estimation of α_b, we evaluated three available kinetic data sets for the highest GA concentration in a way as described for HQ and obtained a median value for $\alpha_b = 0.022$ from an α_b distribution histogram, which is very close to the value obtained for the deliquesced HQ aerosol. Combining α_b obtained from fitting both HQ and GA data sets will lead to $\alpha_b = 0.024^{+0.018}_{-0.003}$ (Figure 7). Running the fitting for all other available experimental data (aerosols 2 to 6) and keeping α_b within the range 0.021−0.042 leads to an estimate of $k_2 = 2.92^{+0.06}_{-0.08} \times 10^8$ L mol^{-1} s^{-1}. Though we cannot distinguish between $k_2(Na_3GA)$ and $k_2(Na_3GA)$, fitting results show no evidence that Na_3GA and Na_2HGA forms have different reactivity. Note that the precision of the estimated k_2 is only valid for the range of α_b values used.

Combining eqs 7 and 10 leads to an expression for γ. As the fits of the model simulation discussed above return the time dependence of $[GA]_b$ for each experiment, γ could be calculated as a function of reaction time (Figure 4, red lines). It is also seen from Figure 4b that in this experiment with relatively low $[GA]_g$, γ decreases with time, which is due to depletion of GA in bulk particle phase. This change is consistent with the changes shown in Figure 6b, where the data indicated deviation from single exponential decay behavior. Values of γ_0 evaluated at time $t = 0$, i.e., valid for the initial reactant concentration, are also listed in Table 2.

From the beginning of our analysis, we have assumed that NO_2 is lost via a bulk reaction in the particles. Overall, as discussed above, we could consistently interpret the time dependent data at different NO_2 concentrations and at different GA concentrations within this framework. If a surface reaction would have been the major pathway, we should have seen a much more significant decrease of uptake due to deactivation of surface molecules. While rapid exchange of reactants between bulk and surface could maintain the surface reactivity, we would expect the reactivity to scale linearly with the condensed-phase reactant concentration at the surface. Already a rough analysis of initial first-order decay rates as those shown in Figure 6 indicates that they scale with the square root of the GA concentration. This indicates that a surface reaction, if present, did not significantly contribute to NO_2 uptake under our conditions, motivating bulk reaction limited kinetics as given in eq 10. This is surprising at first glance as phenolates are known to be surfactants.[52] The reason might be demonstrated by considering the reacto-diffusive length, which is considerable compared to the particle radius in the case of the reaction between NO_2 and GA, especially at lower concentrations of the latter, as mentioned in conjunction with eq 10. Therefore, the observed kinetics is an average over quite a thick surface layer of the particle, within which the average GA concentration is not much different from the normal bulk concentration even if there is some surface excess. Another option to look at this would have been uptake experiments as a function of particle size, which we could not perform.

The confirmation of the rate constant for the reaction of NO_2 with HQ under the conditions of the present experiments, as well as the similarity of the rate constant for GA with those for other hydroxy-substituted aromatic compounds (1.5×10^8 L mol^{-1} s^{-1} for 2-methoxyphenol, 1.3×10^8 L mol^{-1} s^{-1} for 1,2-dihydroxybenzene and 4.5×10^8 L mol^{-1} s^{-1} for 2,6-dimethoxyphenol,[14] 2.1×10^8 L mol^{-1} s^{-1} for 4-methoxyphenol[53]), indicates that the rate constants measured previously in dilute aqueous solutions are transferable to high-ionic strength deliquesced aerosol particles. Our study therefore extends the database for assessing the reactivity of NO_2 with aerosols containing significant amounts of phenolic compounds, such as in biomass burning plumes.[26,54]

Previous estimates for α_b for NO_2 on aqueous surfaces are relatively low (10^{-4} to 10^{-3}).[22,27−30,32,33] The higher value of $\alpha_b = 0.024^{+0.018}_{-0.003}$ is likely due to the fact that in this study we worked with a stronger sink strength in the aqueous phase (higher concentration or reactivity) than the other two studies[29,33] that used a strong aqueous-phase scavenger. On the other hand, the interface of the highly concentrated solution particles may also be different from those of neat aqueous solutions. The higher value for α_b found here underlines that bulk reaction may be the rate-determining step for NO_2 uptake under almost all atmospherically relevant conditions, rather than interfacial mass transport. This means that in practice uptake coefficients for NO_2, calculated using eqs 7 and 10 will remain much lower than α_b, because the bulk-phase kinetics are relatively slow for typical reactant concentrations lower than those used in the present study.

Conclusions and Atmospheric Implications. Using the short-lived radioactive tracer technique, the uptake rates and liquid-phase kinetics of NO_2 with gentisic acid and hydroquinone in deliquesced aerosol particles were investigated for different reactant concentrations. These substances serve as reactants in the reduction of NO_2 to nitrite, which is the liquid-phase base associated to atmospheric nitrous acid. For the interpretation of experimental data, a system of kinetic equations (11) was used, which takes into account depletion of reactant molecules in the particle bulk. A new value for the second-order rate coefficient $k_2 = (2.9 \pm 0.1) \times 10^8$ L mol^{-1} s^{-1} for the reaction between deprotonated dihydroxybenzoic acid (GA) and NO_2 was obtained. The bulk reaction for NO_2 with GA and HQ was fast enough to allow us to estimate the value for the bulk accommodation coefficient to be $\alpha_b = 0.024^{+0.018}_{-0.003}$ from the kinetic experiments. This value is about an order of magnitude higher than previously reported estimates on aqueous surfaces. This higher value of α_b implicates that bulk reaction may be the rate-determining step for NO_2 uptake rather than interfacial mass transport, and the kinetics of the reaction investigated here becomes relevant under atmospheric conditions.

The values for the rate constant obtained in this study should be used to calculate NO_2 uptake to aerosol particles containing significant amounts of phenolic compounds, such as in biomass burning plumes. For the aerosol number and mass concentrations, the fraction of water-soluble organic carbon and chemical composition typical for a young biomass burning smoke plume,[2,54] an estimated phenolate concentration might be up to 10^{-3} mol L^{-1}, resulting in $\gamma \sim 7 \times 10^{-5}$. With initial NO_2 concentration being 20 ppbv, this leads to an estimated nitrite/HONO production rate of initially 30 pptv h^{-1} for an aerosol surface to volume ratio of 6×10^{-4} m^{-1}. A more detailed analysis using a multiphase chemical model coupled to a gas-phase chemical mechanism has shown that this type of reaction is a major source of nitrite/HONO under such conditions,

whereas, e.g., the hydrolysis of NO_2 provides only a negligible contribution.[26] The nitrite/HONO production rate obtained above can be compared with very recently reported in situ HONO production rates of 57 pptv h^{-1} in the free troposphere and of 110 to 180 pptv h^{-1} in the upper boundary layer at noontime, which were calculated to maintain the observed HONO concentrations under photolysis.[55] Photolysis of this HONO can substantially contribute to $^{\bullet}OH$ production in such an environment.[54,55]

Acknowledgment. Technical support by M. Birrer is highly appreciated. K. Stemmler was involved in the preliminary experiments related to this work. We greatly acknowledge the staff of the PSI accelerator facility and of the isotope production facility IP-2. We appreciate the financial support by the Swiss National Science Foundation (grant no. 200020-109341).

References and Notes

(1) Seinfeld, J. H.; Pandis, S. N. *Atmospheric chemistry and physics: From air pollution to climate change*; John Wiley & Sons, Inc.: New York, Chichester, Weinheim, Brisbane, Singapore, Toronto, 1998.

(2) Graham, B.; Mayol-Bracero, O. L.; Guyon, P.; Roberts, G. C.; Decesari, S.; Facchini, M. C.; Artaxo, P.; Maenhaut, W.; Koll, P.; Andreae, M. O. *J. Geophys. Res.-Atmos.* **2002**, doi: 10.1029/2001JD000336.

(3) Rogge, W. F.; Hildemann, L. M.; Mazurek, M. A.; Cass, G. R.; Simoneit, B. R. T. *Environ. Sci. Technol.* **1998**, *32*, 13.

(4) McKenzie, L. M.; Hao, W. M.; Richards, G. N.; Ward, D. E. *Environ. Sci. Technol.* **1995**, *29*, 2047.

(5) Gallet, C.; Keller, C. *Soil Biol. Biochem.* **1999**, *31*, 1151.

(6) Vione, D.; Maurino, V.; Minero, C.; Pelizzetti, E.; Harrison, M. A. J.; Olariu, R. I.; Arsene, C. *Chem. Soc. Rev.* **2006**, *35*, 441.

(7) Khanra, S.; Minero, C.; Maurino, V.; Pelizzetti, E.; Dutta, B. K.; Vione, D. *Environ. Chem. Lett.* **2008**, *6*, 29.

(8) Anastasio, C.; Faust, B. C.; Rao, C. J. *Environ. Sci. Technol.* **1997**, *31*, 218.

(9) Olariu, R. I.; Barnes, I.; Becker, K. H.; Klotz, B. *Int. J. Chem. Kinet.* **2000**, *32*, 696.

(10) Alfassi, Z. B.; Huie, R. E.; Neta, P. *J. Phys. Chem.* **1986**, *90*, 4156.

(11) Miao, J. L.; Wang, W. F.; Pan, J. X.; Lu, C. Y.; Li, R. Q.; Yao, S. D. *Radiat. Phys. Chem.* **2001**, *60*, 163.

(12) Zhan, Z.; Yao, S.; Lin, W.; Wang, W. F.; Jin, Y.; Lin, N. *Free Radical Res.* **1998**, *29*, 13.

(13) Gutzwiller, L.; George, C.; Rössler, E.; Ammann, M. *J. Phys. Chem. A* **2002**, *106*, 12045.

(14) Ammann, M.; Rossler, E.; Strekowski, R.; George, C. *Phys. Chem. Chem. Phys.* **2005**, *7*, 2513.

(15) Alfassi, Z. B.; Huie, R. E.; Neta, P. *J. Phys. Chem.* **1986**, *90*, 4156.

(16) George, C.; Strekowski, R. S.; Kleffmann, J.; Stemmler, K.; Ammann, M. *Faraday Discuss.* **2005**, *130*, 195.

(17) Stemmler, K.; Ammann, M.; Donders, C.; Kleffmann, J.; George, C. *Nature* **2006**, *440*, 195.

(18) Stemmler, K.; Ndour, M.; Elshorbany, Y.; Kleffmann, J.; D'Anna, B.; George, C.; Bohn, B.; Ammann, M. *Atmos. Chem. Phys.* **2007**, *7*, 4237.

(19) Gutzwiller, L.; Arens, F.; Baltensperger, U.; Gaggeler, H. W.; Ammann, M. *Environ. Sci. Technol.* **2002**, *36*, 677.

(20) Hartshorn, M. P. *Acta Chem. Scand.* **1998**, *52*, 2.

(21) Nichols, B. R.; Rapa, C.; Costa, V.; Hinrichs, R. Z. *J. Phys. Chem. C* **2009**, *113*, 2111.

(22) Mertes, S.; Wahner, A. *J. Phys. Chem.* **1995**, *99*, 14000.

(23) Kleffmann, J.; Becker, K. H.; Wiesen, P. *J. Chem. Soc., Faraday Trans.* **1998**, *94*, 3289.

(24) Baker, J.; Ashbourn, S. F. M.; Cox, R. A. *Phys. Chem. Chem. Phys.* **1999**, *1*, 683.

(25) Harrison, R. M.; Peak, J. D.; Collins, G. M. *J. Geophys. Res.-Atmos.* **1996**, *101*, 14429.

(26) Lahoutifard, N.; Ammann, M.; Gutzwiller, L.; Ervens, B.; George, C. *Atmos. Chem. Phys.* **2002**, *2*, 215.

(27) Harrison, R. M.; Collins, G. M. *J. Atmos. Chem.* **1998**, *30*, 397.

(28) Abbatt, J. P. D.; Waschewsky, G. C. G. *J. Phys. Chem. A* **1998**, *102*, 3719.

(29) Msibi, I. M.; Shi, J. P.; Harrison, R. M. *J. Atmos. Chem.* **1993**, *17*, 339.

(30) Cheung, J. L.; Li, Y. Q.; Boniface, J.; Shi, Q.; Davidovits, P.; Worsnop, D. R.; Jayne, J. T.; Kolb, C. E. *J. Phys. Chem. A* **2000**, *104*, 2655.

(31) Kleffmann, J.; Becker, K. H.; Wiesen, P. *Atmos. Environ.* **1998**, *32*, 2721.

(32) Ponche, J. L.; George, C.; Mirabel, P. *J. Atmos. Chem.* **1993**, *16*, 1.

(33) Lee, J. H.; Tang, I. N. *Atmos. Environ.* **1988**, *22*, 1147.

(34) Ammann, M. *Radiochim. Acta* **2001**, *89*, 831.

(35) Vlasenko, A.; Sjogren, S.; Weingartner, E.; Stemmler, K.; Gaggeler, H. W.; Ammann, M. *Atmos. Chem. Phys.* **2006**, *6*, 2147.

(36) Levaggi, D.; Siu, W.; Feldstein, M.; Kothny, E. L. *Environ. Sci. Technol.* **1972**, *6*, 250.

(37) Saltzman, B. E. *Anal. Chem.* **1954**, *26*, 1948.

(38) Guimbaud, C.; Arens, F.; Gutzwiller, L.; Gäggeler, H. W.; Ammann, M. *Atmos. Chem. Phys.* **2002**, *2*, 249.

(39) Kalberer, M.; Tabor, K.; Ammann, M.; Parrat, Y.; Weingartner, E.; Piguet, D.; Rossler, E.; Jost, D. T.; Turler, A.; Gaggeler, H. W.; Baltensperger, U. *J. Phys. Chem.* **1996**, *100*, 15487.

(40) Rogak, S. N.; Baltensperger, U.; Flagan, R. C. *Aerosol Sci. Technol.* **1991**, *14*, 447.

(41) Lide, D. R., Ed. *CRC Handbook of Chemistry and Physics*, 89th ed.; CRC Press: Taylor and Francis, Boca Raton, FL, Internet Version, 2009.

(42) Stahl, P. H. *Handbook of pharmaceutical salts: properties, selection, and use*; Helvetica Chimica Acta; Verlag: Zürich, 2002.

(43) Martinez, N.; Junquera, E.; Aicart, E. *Phys. Chem. Chem. Phys.* **1999**, *1*, 4811.

(44) Patterson, G. S. *J. Chem. Educ.* **1999**, *76*, 395.

(45) Heger, D.; Klanova, J.; Klan, P. *J. Phys. Chem. B* **2006**, *110*, 1277.

(46) Blanco, S. E.; Almandoz, M. C.; Ferretti, F. H. *Spectrochim. Acta Pt. A-Mol. Biomol. Spectrosc.* **2005**, *61*, 93.

(47) Pozdnyakov, I. P.; Sosedova, Y. A.; Plyusnin, V. F.; Grivin, V. P.; Bazhin, N. M. *Russ. Chem. Bull.* **2007**, *56*, 1318.

(48) Fricke, H.; Bartl, K.; Funk, A.; Gerlach, A.; Gerhards, M. *Chemphyschem* **2008**, *9*, 2592.

(49) Poschl, U.; Rudich, Y.; Ammann, M. *Atmos. Chem. Phys.* **2007**, *7*, 5989.

(50) Hanson, D. R.; Ravishankara, A. R.; Solomon, S. *J. Geophys. Res.-Atmos.* **1994**, *99*, 3615.

(51) Huie, R. E.; Neta, P. *J. Phys. Chem.* **1986**, *90*, 1193.

(52) Minofar, B.; Jungwirth, P.; Das, M. R.; Kunz, W.; Mahiuddin, S. *J. Phys. Chem. C* **2007**, *111*, 8242.

(53) Alfassi, Z. B.; Huie, R. E.; Neta, P.; Shoute, L. C. T. *J. Phys. Chem.* **1990**, *94*, 8800.

(54) Alvarado, M. J.; Prinn, R. G. *J. Geophys. Res.-Atmos.* **2009**, *114*, D09306.

(55) Zhang, N.; Zhou, X.; Shepson, P. B.; Gao, H.; Alaghmand, M. ; Stirm, B. , *Geophys. Res. Lett.* **2009**, doi: 10.1029/2009GL038999.

JP9050462